Nonstoichiometric Layered $Li_xMn_yO_2$ with a High Capacity for Lithium Intercalation/Deintercalation

A. Robert Armstrong, Allan J. Paterson, Alastair D. Robertson, and Peter G. Bruce*

School of Chemistry, University of St. Andrews, St. Andrews, Fife KY16 9ST, United Kingdom

Received July 17, 2001. Revised Manuscript Received November 4, 2001

Nonstoichiometric layered $Li_xMn_yO_2$ compounds with the O3 structure (α-$NaFeO_2$ type), space group $R\bar{3}m$, were synthesized by ion exchange from the sodium precursors $Na_xMn_yO_2$. Such lithium intercalation compounds are important in the context of rechargeable lithium batteries since they offer the key advantages of lower cost, lower toxicity, and higher safety when compared with $LiCoO_2$, which is used presently as the positive electrode in these devices. By the varying of the synthesis conditions of the precursor and the ion-exchange process, significant variations of the vacancy content on the transition metal sites could be induced. The variations in composition and defect structure were reflected in differences in the lattice parameters and *hkl* dependent peak broadening, observed in the X-ray diffraction data. Structural details were confirmed by Rietveld refinement using neutron powder diffraction. Lithium intercalation/deintercalation proved very sensitive to the composition and defect structure. High discharge capacities of 190−200 $mAhg^{-1}$ at a rate of C/7 (corresponding to complete discharge in 7 h) could be obtained with a capacity fade of only 0.12% per cycle, at room temperature. This is significantly better than results reported previously for stoichiometric $LiMnO_2$. All of the materials described in this work convert to a spinel-like phase on repeated intercalation/deintercalation of lithium. Such conversion involves the generation of a nanostructured spinel-like phase within each particle. The nanostructure plays a key role in accommodating, at the domain wall boundaries, stresses which normally accompany the first-order Jahn−Teller driven phase transition occurring on cycling in the 3 V region.

Introduction

Rechargeable lithium batteries are now established as one of the major technological developments of the past decade. To achieve a significant advance in this technology it is essential to replace the lithium intercalation compound, $LiCoO_2$, presently used as the positive electrode in such devices, with new materials. Lithium manganese oxides provide, in principle, a particularly attractive alternative because of their significantly lower cost and toxicity compared with $LiCoO_2$ as well as their improved safety. This last issue is critically important for the development of larger lithium-ion cells for high-power applications such as electric vehicles. Since the original report of lithium intercalation into the $LiMn_2O_4$ spinel, this spinel or related spinel materials have been investigated extensively as potential positive electrodes for rechargeable lithium batteries.[1−4] Recently, the synthesis of $LiMnO_2$ with a layered structure similar to that of $LiCoO_2$ has been reported.[5,6] Since then, interest in this intercalation compound has grown rapidly. Layered $LiMnO_2$ has been doped with a variety of other ions including Co, Al, and Ni, and the intercalation chemistry as well as the performance of the materials as positive electrodes have been reported.[7−16] Layered $LiMnO_2$, whether doped or undoped, possesses a structure based on the O3 (α-$NaFeO_2$) type, which consists of close-packed oxide ion layers stacked in an ABC arrangement (cubic close packing) with alternate sheets of octahedral sites between the close-packed oxide layers being occupied by transition metal and alkali ions.

* To whom correspondence should be addressed.

(1) Thackeray, M. M.; David, W. I. F.; Bruce, P. G.; Goodenough, J. B. *Mater. Res. Bull.* **1983**, *18*, 461.
(2) Gummow, R. J.; De Kock, A.; Thackeray, M. M. *Solid State Ionics* **1994**, *69*, 59.
(3) Tarascon, J. M.; McKinnon, W. R.; Coowar, F.; Bowmer, T. N.; Amatucci, G.; Guyomard, D. *J. Electrochem. Soc.* **1994**, *141*, 1421.
(4) Gao, Y.; Dahn, J. R. *J. Electrochem. Soc.* **1996**, *143*, 100.
(5) Armstrong, A. R.; Bruce, P. G. *Nature* **1996**, *381*, 499.
(6) Capitaine, F.; Gravereau, P.; Delmas, C. *Solid State Ionics* **1996**, *89*, 197.
(7) Jang, Y.-I.; Huang, B.; Chiang, Y.-M.; Sadoway, D. R. *Electrochem. Solid-State Lett.* **1998**, *1*, 13.
(8) Armstrong, A. R.; Gitzendanner, R.; Robertson, A. D.; Bruce, P. G. *Chem. Commun.* **1998**, 1833.
(9) Armstrong, A. R.; Robertson, A. D.; Gitzendanner, R.; Bruce, P. G. *J. Solid State Chem.* **1999**, *145*, 549.
(10) Robertson, A. D.; Armstrong, A. R.; Bruce, P. G. *Chem. Commun.* **2000**, 1997.
(11) Robertson, A. D.; Armstrong, A. R.; Fowkes, A. J.; Bruce, P. G. *J. Mater. Chem.* **2001**, *11*, 113.
(12) Quine, T. E.; Duncan, M. J.; Armstrong, A. R.; Robertson, A. D.; Bruce, P. G. *J. Mater. Chem.* **2000**, *10*, 2838.
(13) Ammundsen, B.; Desilvestro, J.; Groutso, T.; Hassell, D.; Metson, J. B.; Regan, E.; Steiner, R.; Pickering, P. J. *J. Electrochem. Soc.* **2000**, *147*, 4078.
(14) Davidson, I. J.; McMillan, R. S.; Slegr, H.; Luan, B.; Kargina, I.; Murray, J. J.; Swainson, I. P. *J. Power Sources* **1999**, *81−82*, 406.
(15) Spohr, M. E.; Novák, P.; Schnyder, B.; Haas, O.; Nesper, R. *J. Electrochem. Soc.* **1998**, *145*, 1113.
(16) Huang, S.-J.; Park, H.-S.; Choy, J.-H. *Chem. Mater.* **2000**, *12*, 1818.

10.1021/cm010382n CCC: $22.00
Published on Web 01/23/2002

The motivation for examining doped, layered, $LiMnO_2$ with the O3 structure was to improve on the performance reported previously for the undoped material. We noted significant improvement in the capacity and its retention on cycling when doped with Co or Ni. However, we also observed that the maximum capacity occurred at relatively low dopant levels: 2.5 and 5 mol % in the case Co and Ni, respectively.[11,12] Synthesis of doped materials by the ion-exchange route resulted in compounds which were nonstoichiometric, with a deficiency in alkali metal and with vacancies on the transition metal sites. Consequently, these nonstoichiometric layered materials possess too low a Mn^{3+} content for promotion of a cooperative Jahn−Teller distortion. As a result, the doped materials exhibit rhombohedral symmetry ($R\bar{3}m$) compared with the previously studied stoichiometric and monoclinic $LiMnO_2$ ($C2/m$). Given that the doped materials differ from stoichiometric $LiMnO_2$ not just in the presence of foreign ions but also in their stoichiometry, defect structure, and symmetry, we were encouraged to investigate undoped and nonstoichiometric layered $Li_xMn_yO_2$.

Experimental Section

$Na_xMn_yO_2$ materials were prepared by mixing Na_2CO_3 (Aldrich 99.5+%) and $Mn(CH_3CO_2)_2{\cdot}4H_2O$ (Aldrich 99+%) in distilled water in the stoichiometric ratio of $x/y = 0.7$. After rotary evaporation, the mixtures were heated in air at 250 °C for 12 h to decompose the acetates. The resulting powder was then fired under a range of conditions. These included temperatures from 450 to 600 °C in air for up to 12 h followed by quenching or slow-cooling. Some samples were subject to a further annealing step in flowing argon. The sodium phases were then ion-exchanged under a range of conditions. The most extreme conditions involved the refluxing in hexanol at 160 °C with a 7−8-fold molar excess of LiBr for up to 8 h. Other conditions involved refluxing in butanol (120 °C), refluxing in ethanol (80 °C), and stirring in ethanol at 25 °C, all with similar levels of excess LiBr. Some of these milder ion-exchange conditions required longer times to achieve completion. After the exchange, the samples were washed in alcohol, water, and finally alcohol again to remove any small amounts of Na_2CO_3 remaining after the high-temperature synthesis of the sodium phase. (As shown later, the Na content of the sodium phase is <0.7).

Chemical analyses for sodium and lithium were carried out by flame emission spectrometry, and that for manganese was carried out by using atomic absorption spectroscopy. The average manganese oxidation state was determined by redox titration using ferrous ammonium sulfate/$KMnO_4$.

Surface area measurements were carried out with the use of the BET method by employing a Micromeritics Gemini 23670 instrument. All samples possessed a surface area in the range of 6−10 m^2g^{-1}.

Powder X-ray diffraction data were collected on a Stoe STADI/P diffractometer operating in transmission mode with Fe $K\alpha_1$ radiation ($\lambda = 1.936$ Å). Compounds of manganese exhibit fluorescence when irradiated by copper X-ray radiation, and although this can be eliminated by using an analyzing monochromator between the sample and the detector, this precludes the use of a primary beam monochromator. By the use of an iron source with a curved germanium monochromator and a small angle position sensitive detector operating in transmission mode, excellent data may be obtained.

Time-of-flight neutron powder diffraction data were obtained on the GEM and Polaris diffractometers at the Rutherford Appleton Laboratory. Since lithium and manganese are neutron absorbers, the data were corrected for absorption before refinement. The structures were refined by the Rietveld method by using the program PRODD based on the Cambridge Crystallographic Subroutine Library (CCSL).[17,18] Scattering lengths of −0.19, −0.373, and 0.5803 (all $\times 10^{-12}$ cm) were assigned to Li, Mn, and O, respectively.[19] Lattice parameters were obtained from X-ray diffraction data by Rietveld refinement using GSAS.[20]

To examine the electrochemical performance of the layered materials, composite electrodes were constructed by mixing the active material, carbon, and Kynar Flex 2801 (a copolymer based on PVDF) in the weight ratio of 85:10:5. The mixture was prepared as a slurry in THF and spread onto aluminum foil using a Doctor Blade technique. After evaporation of the solvent and drying, electrodes were incorporated into an electrochemical cell with a lithium metal counter electrode, and the electrolyte was a 1 molal solution of $LiPF_6$ (Hashimoto) in propylene carbonate (Merck). Electrochemical measurements were carried out using a Biologic MacPile II.

Results and Discussion

$Na_xMn_yO_2$ Materials. The original work on layered lithium manganese oxides involved the synthesis of layered stoichiometric $NaMnO_2$ followed by ion exchange to form the near stoichiometric $LiMnO_2$. Attempts to prepare stoichiometric $LiMnO_2$ doped with other ions proved difficult; however, we found that it was possible to introduce dopants with relative ease provided that compositions deficient in alkali metal ions were employed. Sodium phases, deficient in alkali metal ions and also possessing vacancies on the transition metal sites, could then be ion-exchanged to replace the sodium by lithium. In the present study, we have prepared materials based on the synthesis of alkali metal deficient layered sodium manganese oxides with compositions analogous to the doped materials but without dopants. Attempts to prepare single-phase layered sodium manganese oxides between Na/Mn ratios of 2:3 and 1 proved fruitless: a two-phase mixture of a sodium deficient phase and $NaMnO_2$ was always obtained. Some evidence was, however, found for a narrow range of solid solution around the composition corresponding to a Na/Mn ratio of 2:3. In an earlier study, Parant et al.[21] showed that nonstoichiometric layered sodium phases may be formed depending on the synthesis conditions and these were described by the formula $Na_{0.7}MnO_{2+x}$. The materials were shown to be cation deficient with vacancies on the alkali metal and transition metal sites.[21] These authors also identified a narrow range of composition around a Na/Mn ratio of 2:3. The crystal structure is described as $P3$ with oxygen stacking ABBCC and transition metal ions in octahedral sites with Na^+ in trigonal prismatic coordination. In synthesizing the materials relevant to this publication, we have concentrated on preparing sodium phases in the region where Na/Mn = 2:3. The synthesis conditions for the sodium phases are restricted to temperatures at or below 600 °C since higher temperatures result in the formation of the $P2$ phase. At temperatures significantly below 450 °C, complete reaction does not occur. Within the temperature range of 450−600 °C, we have

(17) Matthewman, J. C.; Thompson, P.; Brown, P. J. *J. Appl. Crystallogr.* **1982**, *15*, 167.
(18) Brown, P. J.; Matthewman, J. C. *Rutherford Appleton Laboratory Report*; RAL-87-010; 1987.
(19) Sears, V. F. *Neutron News* **1992**, *3* (3), 26.
(20) Larson, A. C.; von Dreele, R. B. *General Structure Analysis System*; Los Alamos National Laboratory: Los Alamos, NM, 1995.
(21) Parant, J.-P.; Olazcuaga, R.; DeValette, M.; Fouassier, C.; Hagenmuller, P. *J. Solid State Chem.* **1971**, *3*, 1.

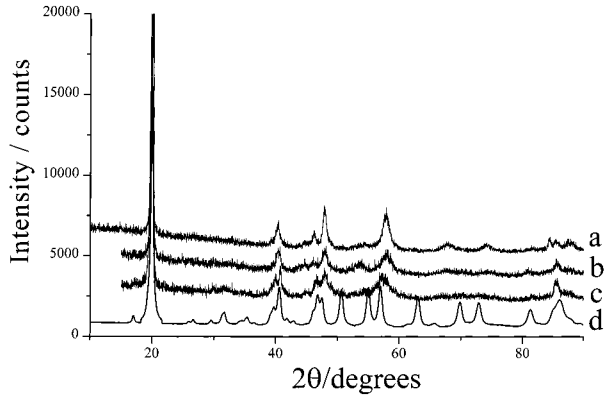

Figure 1. Powder X-ray diffraction patterns (Fe $K\alpha_1$ radiation) for several sodium phases: (a) $Na_xMn_{0.975}Co_{0.025}O_2$, (b) $Na_xMn_yO_2$ quenched from 600 °C, (c) $Na_xMn_yO_2$ slow-cooled from 600 °C, and (d) a simulation of $Na_2Mn_3O_7$.

investigated the varying of the cooling rates and the atmosphere used during synthesis.

The X-ray diffraction patterns obtained for the sodium phases $Na_xMn_yO_2$ generally exhibit broad and somewhat ill-defined peaks. Nevertheless, it is possible to discern a systematic variation in the powder X-ray diffraction patterns with the synthesis conditions. The extremes of behavior are represented by the powder diffraction patterns shown in Figure 1, with one corresponding to a sodium phase prepared at 600 °C with slow cooling and the other using the same temperature but with quenching. The quenched sample has fewer vacancies on the transition metal sites, and these are less ordered than those in the case of the slow-cooled sample. These differences are seen by comparison of the powder diffraction patterns with those obtained from $Na_xMn_{0.975}Co_{0.025}O_2$ and a simulation based on the crystal structure of $Na_2Mn_3O_7$.[22] The former is a quenched phase with a well-defined powder pattern that has been indexed on the *P*3 structure and with disordered transition metal vacancies. The powder pattern for the quenched sodium manganese oxide phase is similar to that of the cobalt-doped material which is consistent with the presence of disordered vacancies on the transition metal sites. In contrast, $Na_2Mn_3O_7$ possesses a layered structure in which the transition metal vacancies are ordered; furthermore, the oxygen stacking sequence is now O3, i.e., all cations are now in octahedral sites. The X-ray diffraction patterns of the slow-cooled layered material possess features that are similar to the pattern for $Na_2Mn_3O_7$ indicating the presence of ordered transition metal vacancies as well as layer stacking that is more akin to O3 than *P*3. The peak broadening present for both the sodium phases prepared in this work suggests that there is no clear demarcation between ordered and disordered vacancies or the different forms of layered stacking. Instead, in the context of the stacking sequence, there is likely to be an intergrowth between *P*3 and O3. A more detailed examination of the vacancy ordering and stacking faults would require investigation by transmission electron microscopy.

Structure of $Li_xMn_yO_2$ Materials. Powder diffraction patterns for a number of layered $Li_xMn_yO_2$ phases

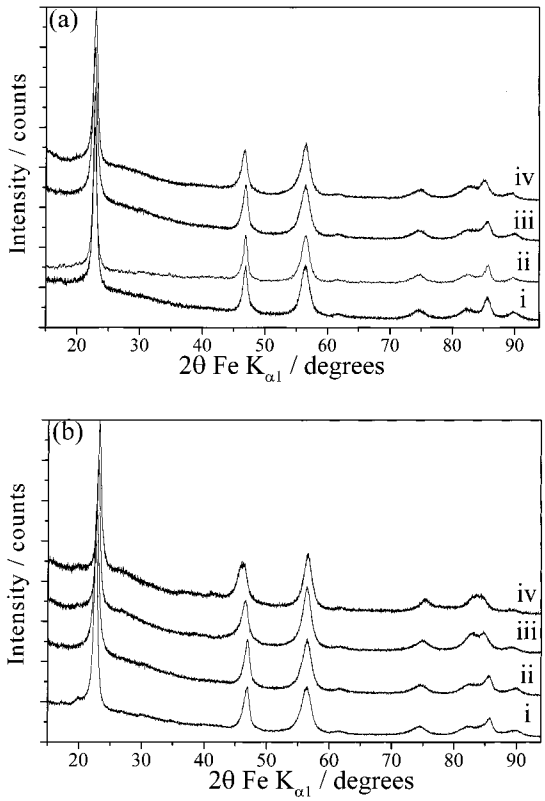

Figure 2. Powder X-ray diffraction patterns (Fe $K\alpha_1$ radiation) for a series of $Li_xMn_yO_2$ phases: (a) Na phases prepared under different conditions and ion-exchanged at 80 °C in ethanol with the material (i) quenched from 450 °C, (ii) slow-cooled from 600 °C, (iii) quenched from 600 °C, and (iv) argon annealed at 600 °C; (b) all Na phases prepared by quenching in air from 600 °C and exchanged at (i) 25 °C in ethanol, (ii) 80 °C in ethanol, (iii) 120 °C in butanol, and (iv) 160 °C in hexanol.

that span a range of synthesis conditions are shown in Figure 2. The powder diffraction patterns for these materials are much better defined than those for the sodium compounds prior to exchange, indicating a significantly higher degree of order. For all the layered $Li_xMn_yO_2$ compounds studied in this work, the powder diffraction data could be indexed on a rhombohedral unit cell, space group $R\bar{3}m$. Evidently, the proportion of Mn^{3+} ions is insufficient to promote a Jahn−Teller distortion in the case of these nonstoichiometric layered lithium manganese oxides and in contrast to stoichiometric $LiMnO_2$. Although all layered lithium phases exhibit rhombohedral symmetry, the lattice parameters do vary to a significant extent depending on the synthesis conditions. These variations are summarized in Figure 3. The hexagonal, *a*, lattice parameter varies from 2.845 Å, in the case of the material in which the sodium precursor was fired at 450 °C and the ion exchange was carried out in ethanol at 80 °C, to a value of 2.877 Å for the material in which the sodium phase was quenched from 600 °C and then exchanged in hexanol at 160 °C. The range of synthesis conditions used to obtain the data reported in Figure 3 is sufficient to permit consideration of how the varying of the synthesis of the sodium phases and the subsequent ion-exchange conditions affects the lattice parameters.

Considering at first changes in the synthesis of the sodium phase, there are several compounds reported for which the ion exchanges were carried out at 80 °C in

(22) Chang, F. M.; Jansen, M. *Z. Anorg. Allg. Chem.* **1985**, *531*, 177.

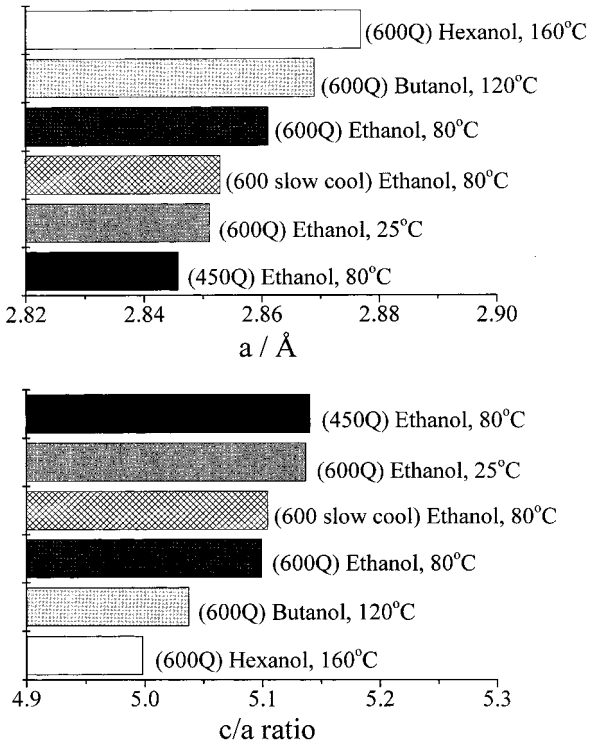

Figure 3. Histograms representing variations in the lattice parameters for $Li_xMn_yO_2$ phases prepared under different conditions: (a) *a* lattice parameter and (b) *c*/*a* ratio. Preparative conditions for the precursor Na phases are shown in parentheses (Q = quenched sample).

ethanol but the sodium precursors were prepared in different ways. The *a* lattice parameter exhibits its smallest value for phases synthesized at 450 °C; a somewhat larger value is observed for materials that were prepared at 600 °C but slow-cooled, and a still larger value is observed for materials that were synthesized at 600 °C and then quenched. The *a* lattice parameter lies in the basal plane of the layered structure and is particularly sensitive to the average Mn−O bond distance. The manganese ions are in two oxidation states: Mn^{4+} ($3d^3$) and Mn^{3+} (high spin $3d^4$). The latter ion is significantly larger than the former (Mn^{4+} = 0.53 Å, Mn^{3+} (HS) = 0.645 Å). The heating of the sodium phases at lower temperatures or slow cooling increases the average oxidation state, reducing the proportion of the larger Mn^{3+} ion with a consequent reduction in the Mn−O bond length and a lowering of the *a* lattice parameter.

We have previously shown that exchange of Na by Li in solutions of LiBr in various alcohols results in the reduction of the material undergoing exchange with associated loss of transition metal vacancies. Furthermore, the reducing conditions can lead to a small degree of lithium intercalation in addition to the ion exchange.[11] Increase in the temperature of the ion exchange results in a greater degree of reduction. The trends in *a* reflect the degree of reduction of the phases during ion exchange. Let us compare the four materials in Figure 3 which were all derived from the same sodium phase prepared at 600 °C and quenched but for which ion exchange was carried out at 25 °C in ethanol, 80 °C in ethanol, 120 °C in butanol, and 160 °C in hexanol. The largest *a* lattice parameter was obtained from the material prepared in hexanol reflecting the greatest degree of reduction (highest Mn^{3+} content), whereas the smallest *a* lattice parameter was obtained from the material prepared in ethanol at room temperature reflecting the lowest Mn^{3+}. Ion exchanges in ethanol at 80 °C and in butanol at 120 °C lie between these two extremes and follow the same trend in *a*. The same variations with synthesis conditions are seen in the *c*/*a* ratios, Figure 3.

Table 1. Compositions and Oxidation States for Various $Li_xMn_yO_2$ Materials. Conditions for Preparation of the Na Phases Are Given in Parentheses (Q = quenched sample).

preparative conditions	calculated composition	avg Mn oxidn state
Na phase (600 °C Q)	$Na_{0.51}Mn_{0.90}O_2$	3.88+
(450 °C Q); ethanol, 80 °C	$Na_{0.070}Li_{0.50}Mn_{0.93}O_2$	3.68+
(600 °C Slow Cool); ethanol, 80 °C	$Na_{0.048}Li_{0.57}Mn_{0.93}O_2$	3.64+
(600 °C Q); ethanol, 25 °C	$Na_{0.068}Li_{0.53}Mn_{0.94}O_2$	3.62+
(600 °C Q); ethanol, 80 °C	$Na_{0.069}Li_{0.59}Mn_{0.94}O_2$	3.55+
(600 °C Ar anneal); ethanol, 80 °C	$Na_{0.056}Li_{0.57}Mn_{0.95}O_2$	3.55+
(600 °C Q); butanol, 120 °C	$Na_{0.056}Li_{0.77}Mn_{0.91}O_2$	3.49+
(600 °C Q); Hexanol, 160 °C	$Na_{0.035}Li_{0.61}Mn_{1.01}O_2$	3.32+

Detailed composition and oxidation state analyses have been carried out on a range of nonstoichiometric $Li_xMn_yO_2$ phases which vary in the synthesis of the sodium phases and in the ion-exchange conditions: Table 1. Examination of these results indicates that the majority of the sodium is replaced by lithium with a residual Na content between 4 and 7%. It is observed that the amount of residual Na in the pure Mn compounds is greater after ion exchange than that in materials doped with, for example, Co or Ni for which more complete exchange was obtained.[11,12] This is presumably due to the higher concentration of vacancies present in the sodium phase of the pure Mn compounds. The presence of vacancies on the transition metal sites for most of the synthesis conditions explored in this work is confirmed in Table 1. The vacancy content approaches 10% before exchange and is reduced in varying degrees by ion exchange to a value of 0 in the case of samples prepared in hexanol. The general trends in the variation of oxidation state with synthesis conditions reflect those determined by considering the variation of the *a* lattice parameter, as described above. The compound prepared at 450 °C and then ion-exchanged at 80 °C in ethanol exhibits one of the highest oxidation states, whereas the material quenched at 600 °C and then exchanged in hexanol exhibits the lowest oxidation state. In the comparison of the material quenched at 600 °C and exchanged at 25 °C in ethanol with the sample prepared by slow cooling from 600 °C and the exchange at 80 °C in ethanol, the *a* lattice parameters and the oxidation states are very similar, Figure 3 and Table 1, indicating that the greater oxidation of the Na phase obtained by slow cooling compared with quenching is balanced by the greater reduction at 80 °C than at 25 °C.

At first sight, the results for butanol reported in Table 1 seem anomalous and deserve special consideration. As discussed above and previously, during ion exchange in alcohols, two processes are possible in addition to the exchange itself: reduction of the transition metal oxide sub-lattice with elimination of vacancies and intercalation of lithium. The degree to which vacancies are eliminated or lithium ions are intercalated depends on

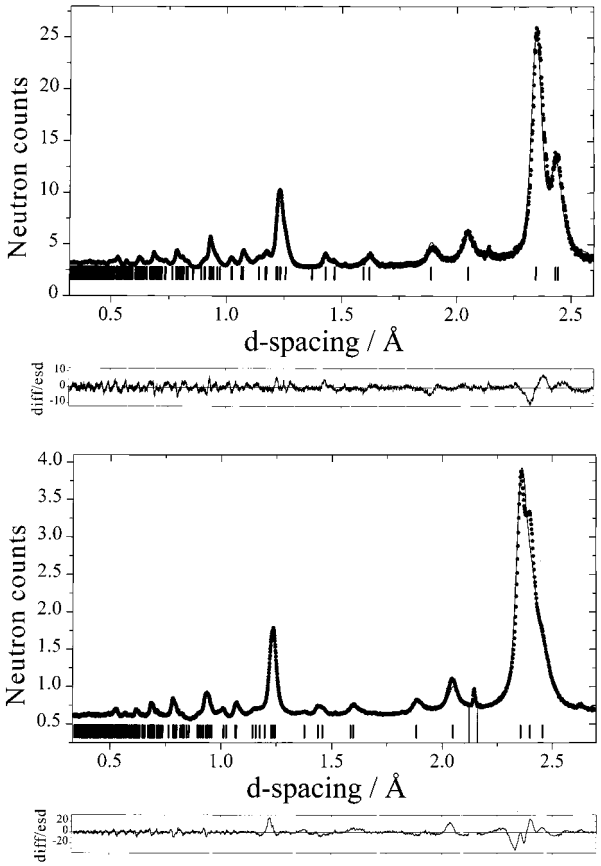

Figure 4. Fit to powder neutron diffraction data for two Li_x-Mn_yO_2 materials: (a) Na precursor quenched from 600 °C and ion-exchanged under reflux in ethanol at 80 °C and (b) Na precursor quenched from 600 °C and ion-exchanged under reflux in hexanol at 160 °C. Dots (●) represent observed data and solid line represents the calculated pattern. Tick marks show positions of allowed reflections. Lower box shows difference/esd.

Table 2. Structured Parameters for Two Layered $Li_xMn_yO_2$ Phases: (a) Sodium Phase Quenched from 600 °C and Exchanged in Ethanol at 80 °C; (b) the Same Sodium Phase but Exchanged in Hexanol at 160 °C

atom	Wyckoff symbol	*x/a*	*y/a*	*z/c*	B_{iso}	occupancy
			(a) Space group $R\bar{3}m$[a]			
Li/Na	3b	0.0	0.0	0.5	1.0	0.69(2)/0.07
Mn	3a	0.0	0.0	0.0	0.76(3)	0.94
O1	6c	0.0	0.0	0.26153(5)	0.74(1)	1
			(b) Space group $R\bar{3}m$[b]			
Li/Na	3b	0.0	0.0	0.5	0.4(3)	0.67(2)/0.035
Mn	3a	0.0	0.0	0.0	0.64(11)	1
O1	6c	0.0	0.0	0.2600(2)	0.48(1)	1

[a] $a = 2.8608(3)$ and $c = 14.5877(18)$ Å. $R_{exp} = 1.0\%$, $R_{wp} = 2.1\%$, and $R_P = 3.4\%$. [b] $a = 2.8769(6)$ and $c = 14.380(3)$ Å. $R_{exp} = 0.7\%$, $R_{wp} = 3.4\%$, and $R_P = 2.6\%$.

the relative kinetics of these two processes. Whereas, at 160 °C in hexanol, there is substantial reduction of the transition metal oxide sub-lattice and elimination of vacancies; the conditions present in butanol at 120 °C appear to favor lithium intercalation. We speculate that a proportion of this excess lithium is likely to be accommodated in the vacant transition metal sites so that, in fact, there are far fewer vacancies on the transition metal sites than would be the case if only manganese occupied the sites.

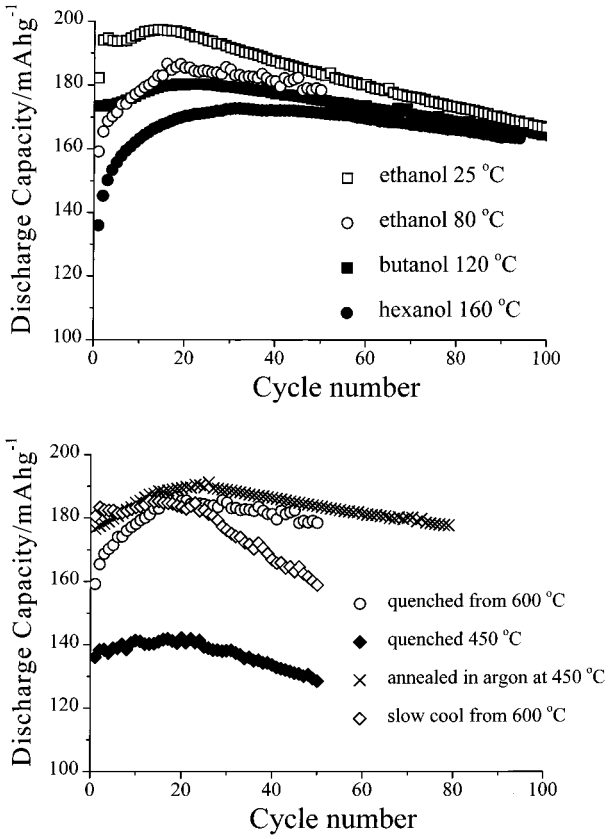

Figure 5. Discharge capacity as a function of cycle number for $Li_xMn_yO_2$ (rate = 25 mAg^{-1}, potential limits = 2.5−4.6 V): (a) Na precursor quenched from 600 °Cand ion-exchanged under different conditions and (b) Na precursor prepared under various conditions and ion-exchanged under reflux in ethanol at 80 °C. Note that results for the material prepared at 600 °C, quenched, and ion-exchanged at 80 °C in ethanol are presented in both (a) and (b) to aid comparison.

Examination of the powder X-ray diffraction data in Figure 2 reveals that, in addition to the variation in lattice parameters, the different synthesis conditions lead to differences in the degree of *hkl* dependent peak broadening and to the relative intensities in the region of 80−95° in 2θ (Fe $K\alpha_1$). The data in Figure 2 are divided into two groups. Figure 2a presents results for the materials that were ion-exchanged at 80 °C in ethanol but for which the sodium precursor phases were synthesized in different ways. Figure 2b presents the variations obtained for phases ion-exchanged in different ways but for which the sodium phase was prepared by quenching from 600 °C. In both cases, the *hkl* dependent peak broadening is most prevalent in the highly oxidized samples. The intensities of the 108 and 110 reflections also differ to a greater extent in the highly oxidized samples, although in this case, the differences are more pronounced in Figure 2b. The nature of the *hkl* dependent peak broadening is the same as we observed previously for the Co-doped layered materials.[11] Its origin lies in stacking faults in the *c*-axis direction arising from ordering of the residual Na^+ ions. Such stacking faults are likely to be the main cause of the intensity differences observed between 80 and 95° in 2θ. Since the vacancies on the transition metal sites carry an effective negative charge, it is possible that they trap some Na^+ ions resulting in the observed incomplete exchange of Na by Li (Table 1). The

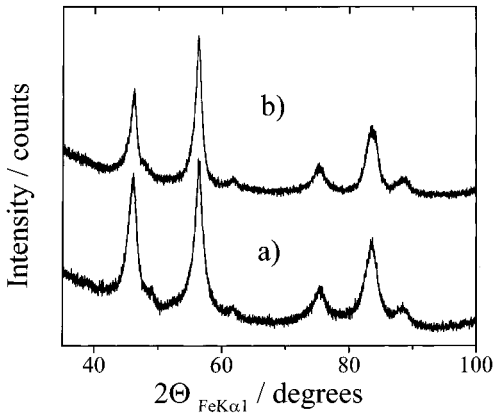

Figure 6. X-ray diffraction patterns (Fe Kα radiation) for two different layered phases after conversion to spinel-like materials on cycling: (a) Na precursor quenched from 600 °C and ion-exchanged under reflux in hexanol at 160 °C after 70 cycles and (b) Na precursor quenched from 600 °C and ion-exchanged at 25 °C in ethanol after 70 cycles.

ordering of the transition metal vacancies may also occur due to their interaction with the Na^+ ions. However, a more detailed consideration of these phenomena would require studies using high-resolution electron microscopy.

The structure of the layered nonstoichiometric Li_x-Mn_yO_2 phases was investigated by neutron powder diffraction. Rietveld refinement was carried out by using a model based on the O3 structure in which the Mn and alkali metal ions occupy alternate sheets of octahedral sites between the close-packed oxide ion layers. During the refinement, occupancy of the transition metal sites (3a) of space group $R\bar{3}m$ was fixed at a value determined from the compositional analysis whereas the occupancy of the 3b sites by Li^+ was allowed to vary freely. The residual Na was also fixed at a value corresponding to the Na content obtained by chemical analysis. Samples synthesized in several different ways were investigated. Two examples are shown in Figure 4. In the case of the material quenched from 600 °C and then ion-exchanged in ethanol at 80 °C, the fit is excellent, whereas the material prepared in hexanol at 160 °C gave rise to a neutron powder diffraction pattern which was not well-described by the above model, although the fit was still satisfactory. The crystallographic data obtained from these fits is presented in Table 2. It may be noted that removal of the triple peak above 2.25 Å in the case of the data in Figure 4b did not alter the structural model obtained on refinement. The fact that the refined lithium occupancies were in reasonable agreement with the values expected from the composition analysis supports the proposed structural model.

Electrochemistry. The variation of discharge capacity with cycle number for layered $Li_xMn_yO_2$ materials prepared under a variety of conditions is shown in Figure 5. The results presented in Figure 5a correspond to phases quenched from 600 °C and ion-exchanged in different ways, whereas Figure 5b presents results from materials that were ion-exchanged at 80 °C in ethanol but for which the precursor sodium phases were synthesized under different conditions. Despite the fact that all the compounds reported in Figure 5a possess the same basic layered rhombohedral structure, the variations in performance are significant, serving to emphasize how sensitive the cycling performance is to the defect chemistry of the materials. The highest initial capacity is obtained for the material quenched in air from 600 °C and ion-exchanged in ethanol at room temperature. The lowest discharge capacity is delivered by the material prepared at 450 °C and ion-exchanged in ethanol at 80 °C. Although it is not possible to give a detailed interpretation of the variations in discharge capacity with cycle number for each material, some general trends do emerge. As has been demonstrated previously for layered lithium manganese oxides doped with Co, Ni, Al, etc., all the $Li_xMn_yO_2$ phases convert to

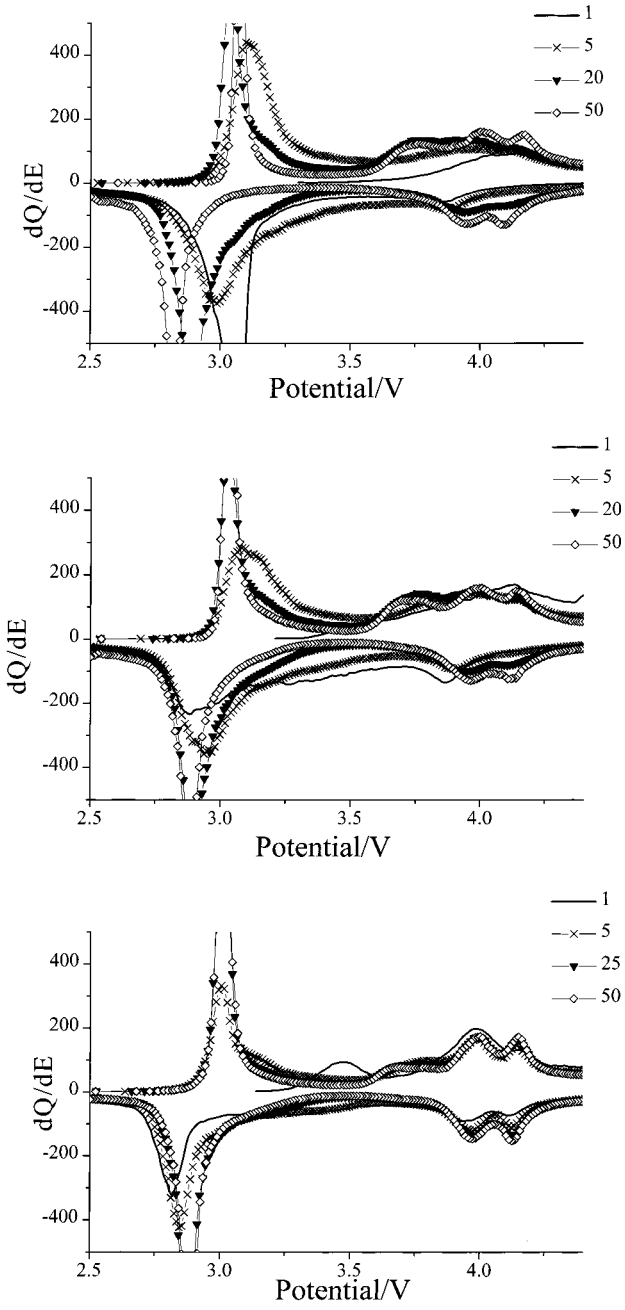

Figure 7. Incremental capacity plots for $Li_xMn_yO_2$ materials showing effect of ion-exchange conditions on rate of conversion to a spinel-like phase: (a) Na precursor slow-cooled from 600 °C and ion-exchanged in ethanol at 80 °C, (b) Na precursor quenched from 600 °C and ion-exchanged in butanol at 120 °C, and (c) Na precursor quenched from 600 °C and ion-exchanged in hexanol at 160 °C. Cycling was carried out at 25 mAg^{-1}.

a spinel-like structure on cycling. As shown in Figure 7 and discussed in greater detail later, conversion to spinel is commenced within the first cycle for highly reduced materials (e.g., synthesized by quenching from 600 °C and ion-exchanged in hexanol at 160 °C) whereas the more oxidized materials (e.g., slow-cooled from 600 °C and refluxed in ethanol at 80 °C) show little evidence of spinel-like phase until some 20−30 cycles. As a result, it is useful to divide the discharge curves in Figure 5 into two regions: region 1 spans cycle numbers from 0 to 20−30 and region 2 corresponds to data above 20−30 cycles.

Considering first capacities up to cycles 20/30, the observed values are not limited by the theoretical capacities to insert lithium ions and electrons into the different materials. Instead, the discharge capacities are limited by kinetics. This is evident from Figure 8 where the discharge capacities in this region decrease significantly with increasing rate. In fact, the shape of the discharge curve for the material prepared at 600 °C, quenched, and ion-exchanged at 25 °C in ethanol (Figure 8a) changes dramatically at 100 mAg^{-1} so that it displays a rise more typical of the material prepared at 600 °C and exchanged in hexanol and cycled at 25 mAg^{-1}. If we consider Figure 5a in particular, it is evident that the conversion of the reduced samples (e.g., 600 °C, hexanol 160 °C) to spinel has a deleterious effect on the kinetics whereas the more oxidized material (e.g., 600 °C quenched, ethanol 25 °C) not only cycles well over the first few cycles, when the structure is predominantly layered, but also appears to accommodate the transformation to spinel in a relatively facile manner.

Considering now region 2, i.e., above cycle 30, it may be noted that the lowest fade rates appear to be associated with the more reduced samples, for example, the materials quenched from 600 °C and ion-exchanged in hexanol or butanol. The fade is also relatively low for the material annealed in argon and ion-exchanged at 80 °C in ethanol. In contrast, the fade rate is high for materials that are slow-cooled from 600 °C and exchanged in ethanol at 80 °C.

Examination of the results in Figure 5a indicates a certain convergence of the capacities for materials in which the sodium phases were prepared in the same way but ion exchange was carried out under different conditions. This seems surprising at first sight since the different ion-exchange conditions induce different degrees of reduction and intercalation of lithium. Given the differences in the average oxidation state of manganese and the variations in the occupancy of the transition metal sites by manganese ions, different spinel-like phases might have been expected on cycling. Examination of X-ray diffraction patterns after cycling for materials prepared in different ways indicates that the lattice parameters converge (Figure 6). Hence, the convergence of discharge capacity is matched by convergence in the lattice parameters of the cycled materials, indicating that further changes in the defect chemistry of the materials occur on cycling rendering the materials and hence their performance the same. As we shall see later, the nanostructures developed for materials prepared under different ion-exchange conditions are similar, further reinforcing the convergence.

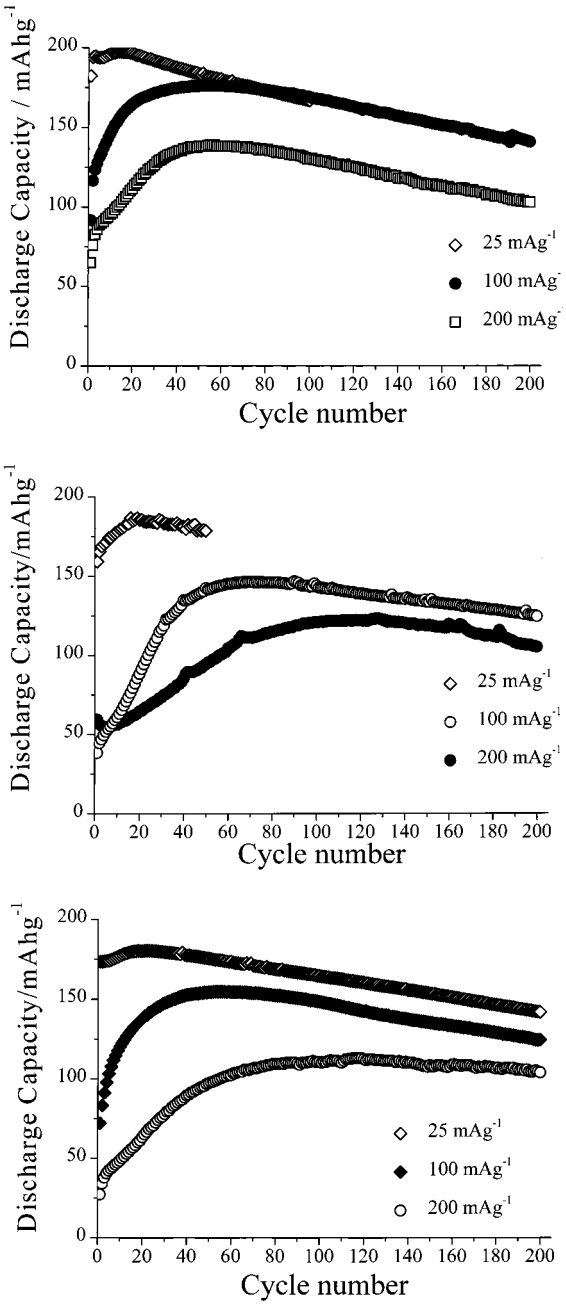

Figure 8. Discharge capacity as a function of cycle number at rates of 25 mAg^{-1}, 100 mAg^{-1}, and 200 mAg^{-1} for $Li_xMn_yO_2$ (potential limits = 2.5−4.6 V): (a) Na precursor quenched from 600 °C and ion-exchanged in ethanol at 25 °C, (b) Na precursor quenched from 600 °C and ion-exchanged in ethanol at 80 °C, and (c) Na precursor quenched from 600 °C and ion-exchanged in butanol at 120 °C.

It is noteworthy that despite the different layered materials converting to phases with diffraction patterns that somewhat resemble spinel with similar lattice parameters it is not possible to conclude that the materials become cubic. On fitting a layered ($R\bar{3}m$) lattice to the XRD data, the *c*/*a* ratio remains significantly greater than 4.9. Therefore, although there is a reduction of *c*/*a* ratios on cycling and a progression toward a cubic lattice (*c*/*a* = 4.9), this value is not reached at least up to 100 cycles. The situation is further complicated by the breadth of the peaks; however, even by taking this into account, the materials remain noncubic. It is for this reason that the term spinel-like

is used throughout the present paper, recognizing that there are differences between these materials and a regular cubic spinel with the ideal distribution of ions.

Conversion from a layered to a spinel-like phase is evident in the incremental capacity plots for the $Li_xMn_yO_2$ materials, Figure 7. The characteristic signal of spinel, two pairs of peaks in the region of 3.9−4.1 V vs Li^+ (1M)/Li, developed more slowly in the case of highly oxidized materials with a large number of vacancies on the transition metal sites. For example, in the case of the material slow-cooled from 600 °C and ion-exchanged in ethanol at 80 °C, a significant spinel signature appears after about 30 cycles (Figure 7a). In contrast, the material quenched from 600 °C and exchanged in hexanol at 160 °C shows evidence of a spinel-like phase even in the first cycle (Figure 7c). The compound prepared in butanol at 120 °C exhibits a rate of conversion to a spinel-like phase that lies between the ethanol and hexanol samples. Comparison of the conversion rate with the *c*/*a* ratios of the original layered phases suggests that the closer the *c*/*a* ratio is to 4.9 (the value corresponding to a cubic lattice) the more rapid is the conversion to a spinel-like phase.

The rate capability of the materials is particularly important in the context of their potential use as positive electrodes in rechargeable lithium batteries. The discharge capacities as a function of cycle number at three different rates, 25 mAg^{-1} (∼C/7), 100 mAg^{-1} (∼2/3 C), and 200 mAg^{1-} (∼1.5 C), are shown in Figure 8 for layered $Li_xMn_yO_2$ materials prepared under several different conditions. In all cases, there is significant reduction in the discharge capacity with increasing rate during the early stages of cycling. This may be attributed to the structural changes that commence during these early cycles.[29] The trends observed in the data obtained on cycling at high rate reflect those observed for lower rate cycling and reported in Figure 5. The compounds quenched from 600 °C and exchanged in ethanol at room temperature exhibit capacities exceeding those of samples exchanged in ethanol at 80 °C and cycled at the same rates. The capacity fade at higher cycle number is again somewhat greater for the more oxidized samples, e.g., ion exchange at room temperature compared with butanol at 120 °C.

Although the primary purpose of the present paper is to report the performance of nonstoichiometric layered $Li_xMn_yO_2$ as a cathode material, it is interesting to compare the performance of this material with those of layered lithium manganese oxides doped using Co and Ni reported by us previously.[10−12] The comparison is especially interesting since the Co- and Ni-doped materials are also deficient in lithium and possess vacancies on the transition metal sites. In our studies of the $Li_xMn_yO_2$ compounds and the related doped materials, we have explored a variety of ion-exchange conditions. For comparison, we shall focus on the materials exchanged at 80 °C in ethanol. They all possessed the same layered $R\bar{3}m$ structure and have a similar number of transition metal vacancies. All have been cycled at 25 mAg^{-1} and between the same voltage limits of 2.4−4.6 V. Consistently, it is found that the initial discharge capacity is about 10−20 $mAhg^{-1}$ higher for the doped materials. When comparisons are made at higher rates, the differences between doped and undoped materials

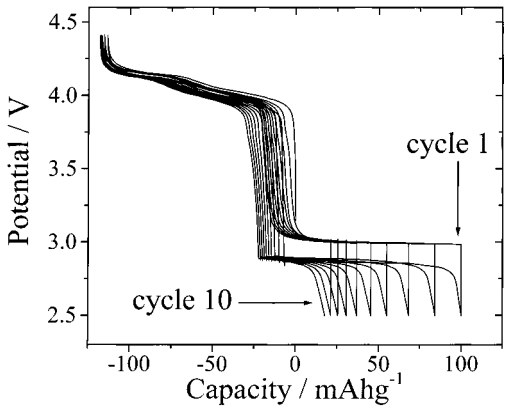

Figure 9. Variation of potential with state of charge on cycling lithium-doped $Li_{1.07}Mn_{1.93}O_4$ spinel prepared by high-temperature solid-state reaction.

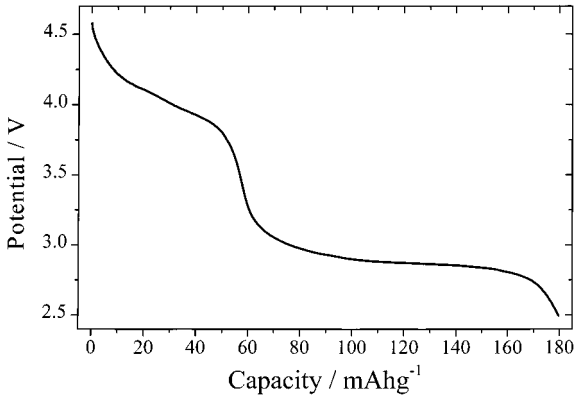

Figure 10. Discharge potential as a function of the state of charge on the 50th cycle for $Li_xMn_yO_2$ for which the Na precursor was fired at 600 °C, quenched, and exchanged at 80 °C in ethanol. Rate = 25 mAg^{-1}.

are even more pronounced. The precise role of dopants in enhancing performance and the comparison between different dopants will be addressed in more detail in a subsequent publication.

Origin of Capacity Retention on Cycling. It is well-known that regular $LiMn_2O_4$ spinel prepared at high temperature, whether it is stoichiometric or is doped with, for example, lithium, exhibits severe capacity fade when cycled over a wide voltage range that incorporates both the 3 and 4 V plateaux. Often such capacity fade has been attributed to the breakup of particles with the consequent loss of contact induced by the sudden and anisotropic expansion which occurs at 3 V due to the formation of the tetragonal phase. However, if this were so, the capacity would be lost in equal measure from the 3 and 4 V regions, which is not the case. This is especially evident with lithium-doped spinel which continues to cycle quite well over the 4 V plateau but rapidly loses capacity in the 3 V region (Figure 9). The capacity fade is related to the Jahn−Teller distortion and hence associated in some way with the first-order phase transition between cubic and tetragonal spinel when cycled over the 3 V plateau, but it is not a straightforward issue of electrochemical grinding.

The materials described in this paper convert to a spinel-like structure but exhibit far superior capacity retention than the regular (high temperature) spinels when cycled over a wide voltage range that incorporates

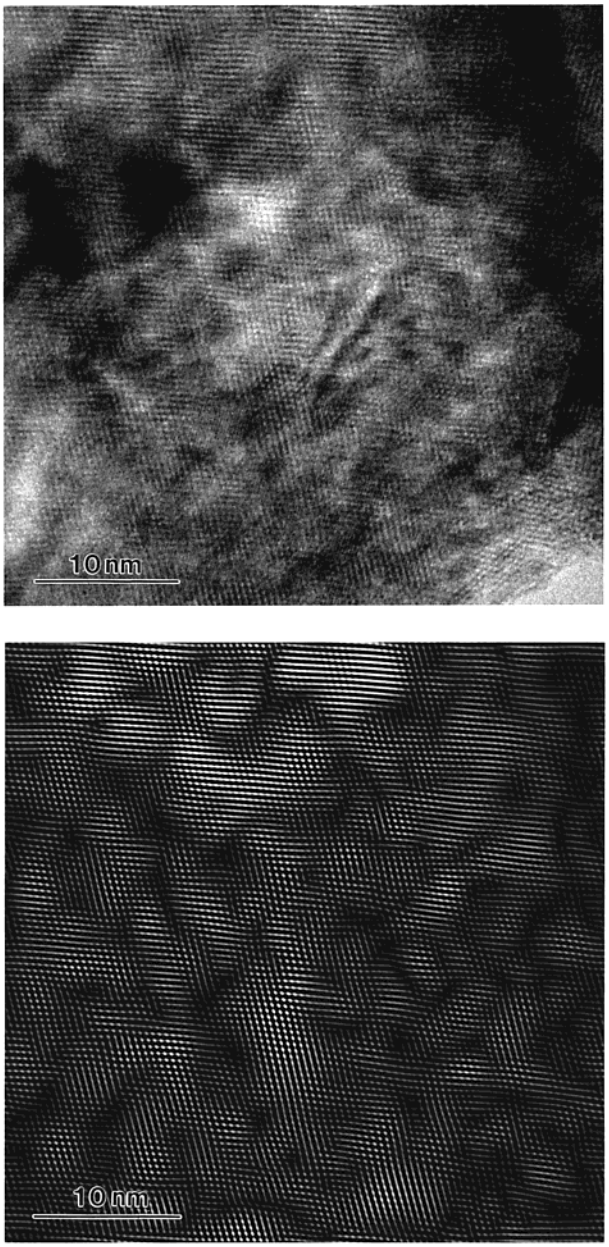

Figure 11. High-resolution electron micrograph of a $Li_xMn_yO_2$ phase after conversion to a nanostructured spinel-like material: (a) bright field image and (b) Fourier filtered image highlighting the domain wall boundaries (dark regions).

both the 3 and 4 V plateaux. Indeed, far from losing capacity at 3 V, most of the capacity obtained from these materials continues to be delivered on a plateau at this potential (Figure 10). On insertion of lithium into regular spinel at 3 V, the tetragonal phase is formed and a cubic/tetragonal phase boundary moves across the particles. The tetragonal phase possesses a volume which is approximately 6% larger than the cubic phase; however, of greater importance is the fact that the expansion is anisotropic with a *c*/*a* ratio for the tetragonal phase of 1.16. Such a transformation establishes strain in the crystallites. We have shown previously, based on electrochemical and structural data, that when layered lithium manganese oxides convert to a spinel-like phase they do so by generating a nanostructure within the particles.[23−25] The original particles remain largely intact and continue to be of micrometer dimensions, but within them they contain a mosaic or a nanodomain structure. This nanodomain spinel-like structure may be directly observed by high-resolution electron microscopy (Figure 11). A similar structure has been observed when orthorhombic $LiMnO_2$ converts to spinel on cycling and for aluminum-doped layered materials.[26,27] These authors have also discussed the crystallography of the transformations. Now, on insertion of lithium into the spinel-like material, the small domains, typically with dimensions of around 60 Å, can transform themselves between the undistorted and distorted phases with the strain of the transformation being accommodated by slippage at the domain wall boundaries. As a result, the first-order phase transformation between undistorted and Jahn−Teller distorted materials is rendered far more facile than that in the absence of nanostructuring, i.e., for regular spinel. This concept has been recently further reinforced by the grinding of regular spinel, which induces a nanostructure and substantially improves cycling in the 3 V region.[28] We have shown that the $Li_xMn_yO_2$ phases prepared under different reflux conditions and possessing different compositions, lattice parameters, and different numbers of defects converge in their electrochemical behavior on extended cycling (Figure 5a). This is not only associated with a convergence in their lattice parameters but is also reflected in the fact that the nanostructures are similar. Therefore, there is good correlation between the convergence of performance, structure, and nanostructure.

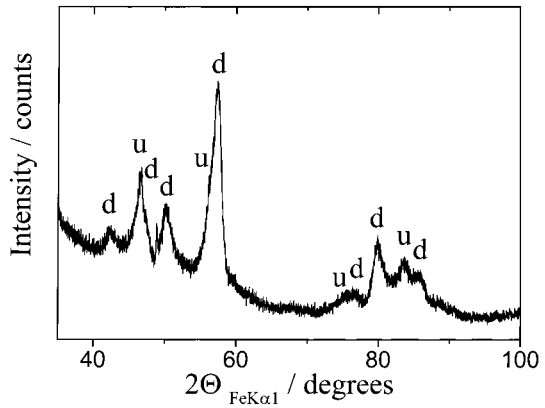

Figure 12. X-ray diffraction pattern (Fe $K\alpha_1$ reduction) for $Li_xMn_yO_2$ (600 Q, 80 °C ethanol) after 70 cycles and at the end of discharge. Two phases corresponding to the undistorted (u) and Jahn−Teller distorted (d) materials are evident.

A very high degree of reversibility is essential for an intercalation reaction if it is to be utilized as the basis of an electrode in an electrochemical cell. Conventional thinking has it that intercalation must be accompanied by near zero expansion and certainly phase changes

(23) Bruce, P. G.; Armstrong, A. R.; Gitzendanner, R. L. *J. Mater. Chem.* **1999**, *9*, 193.
(24) Shao-Horn, Y.; Hackney, S. A.; Armstrong, A. R.; Bruce, P. G.; Gitzendanner, R.; Johnson, C. S.; Thackeray, M. M. *J. Electrochem. Soc.* **1999**, *146*, 2404.
(25) Robertson, A. D.; Armstrong, A. R.; Bruce, P. G. *Chem. Mater.* **2001**, *13*, 2380.
(26) Wang, H.; Jang, Y. I.; Chiang, Y. M. *Electrochem. Solid-State Lett.* **1999**, *2*, 490.
(27) Chiang, Y. M.; Wang, H.; Jang, Y.-I. *Chem. Mater.* **2001**, *13*, 53.
(28) Kang, S.-H.; Goodenough, J. B.; Labenberg, L. K. *Chem. Mater.* **2001**, *13*, 1758.

should be avoided. It has now been shown that by the nanostructuring of an intercalation compound, reversibility in the intercalation process of 99.9% may be obtained despite passage through a first-order Jahn−Teller driven phase transition on each cycle. Such nanostructuring is not confined to the materials described here and could in principle be applied to other intercalation reactions. Note that the compounds are not nanoparticulate but nanostructured. Nanoparticles would lead to a high surface area with consequences for capacity fade because of the catalytic nature of the manganese oxide surface toward electrochemical oxidation.

It has been suggested that cycling may induce migration of some manganese ions into the tetrahedral 8a sites (spinel nomenclature) leading to a reduction of the Jahn−Teller distortion.[27,29] We do not rule out the possible role that this may also have in facilitating the cycling. However, as demonstrated in Figure 12, two phases exist on cycling so that there is no doubt that a first-order Jahn−Teller driven phase transition persists.

Acknowledgment. P.G.B. is indebted to the EPSRC and The Royal Society for financial support. The authors would also like to thank M. J. Duncan and M. J. Forrest for help with the HREM measurements.

CM010382N

(29) Reed, J.; Ceder, G.; van der Ven, A. *Electrochem. Solid-State Lett.* **2001**, *4*, 78.